



Removal of Heavy Metals: Pb(II), Ni(II), and Cd(II) by Fe₃O₄@SiO₂-TMPDT Adsorbent Prepared from Rice Husk Ash

Sri Hastuti*, Tri Martini, Atmanto Heru Wibowo, Dina Fitriana, Wihda Zuhara, Hesti Mutma'inah, Rima Indriyana Putri

Department of Chemistry, Faculty of Mathematics and Natural Sciences, Universitas Sebelas Maret
 Jalan Ir. Sutami 36 A, Kentingan, Surakarta, 57126, Indonesia

*Corresponding author: srihastuti71@staff.uns.ac.id

DOI: [10.20961/alchemy.21.1.91934.53-63](https://doi.org/10.20961/alchemy.21.1.91934.53-63)

Received 8 August 2024, Revised 7 October 2024, Accepted 18 October 2024, Published 28 March 2025

Keywords:

adsorption;
 heavy metal ions;
 rice husk ash;
 silica;
 TMPDT.

ABSTRACT. The adsorption of Pb(II), Ni(II), and Cd(II) metal ions onto Fe₃O₄@SiO₂-TMPDT adsorbent was carried out through batch experiments. In this study, Fe₃O₄@SiO₂-TMPDT adsorbent was synthesized through a sol-gel process using sodium silicate extracted from rice husk ash (Na₂SiO₃)_{RHA} with the addition of magnetite (Fe₃O₄) and modifier N¹-(3-trimethoxysilylpropyl) diethylenetriamine (TMPDT). The synthesized adsorbent was then characterized by FTIR. The Fe₃O₄@SiO₂-TMPDT adsorbent was prepared with suspension Fe₃O₄:(Na₂SiO₃)_{RHA} ratios (v/v) of 1:4, 2:3, and 1:1, and varying the amounts of TMPDT of 1; 2.5 and 5 mL. The optimum pH to perform conditions adsorption for Pb(II) metal ions was determined to be 4, while Ni(II) and Cd(II) were 5. In addition, the adsorption process followed a pseudo-second-order kinetic model, and the adsorption isotherm was consistent with the Langmuir isotherm. The adsorption capacities for Pb(II), Ni(II), and Cd(II) were 11.760 mg/g, 1.864 mg/g, and 1.888 mg/g, respectively.

INTRODUCTION

Groundwater is a clean water source for human consumption, and its contamination may arise from various pollutant origins, such as industrial and anthropogenic activities (Javaheri *et al.*, 2019). Heavy metals, such as Cr, Hg, Cd, Ni, Zn, Mn, Cu, Fe, and Pb, are very harmful to the environment because of their toxic, cumulative, and non-degradable nature (Dong *et al.*, 2015; Hajiaghababaei *et al.*, 2011; Naat *et al.*, 2021; Namasivayam and Ranganathan, 1995; Tang *et al.*, 2013; Yuan and Liu, 2013; Zhou *et al.*, 2014). The metal ion poisoning of Pb(II) causes language difficulties, mental retardation, and abnormalities in pregnant women, kidney problems, anemia, and digestive disorders, such as vomiting and stomach ulcers (Awual *et al.*, 2014; Hajiaghababaei *et al.*, 2011; Huang *et al.*, 2018; Naat *et al.*, 2021; Yuan and Liu, 2013). Similarly, the disorders caused by Ni(II) metal ions include cancer of the lungs and kidney, headache, dizziness, nausea, vomiting, chest pain, coughing, shortness of breath, cyanosis, and weakness (Azimi *et al.*, 2017; Thakur and Parmar, 2013; Zhou *et al.*, 2014). Cd(II) metal ion poisoning damages the physiological systems of the body, leading to long-term accumulation in the human organs, specifically the kidneys and liver (Hajiaghababaei *et al.*, 2011; Javaheri *et al.*, 2019). According to the 2023 Regulation of the Minister of Health RI No. 2 concerning Environmental Health, the quality standard for Pb(II), Ni(III), and Cd(II) metal ions for drinking water is 0.01, 0.07, and 0.003 mg/L, respectively. The metal content of Pb(II), Ni(II), and Cd(II) in drinking water must not exceed the quality standard (Minister of Health Regulation Number 2, 2023).

Rice husk is a byproduct of agricultural waste, and its production worldwide reaches 120 million tons annually (Bheel *et al.*, 2018). The combustion of rice husk converts it into ash containing 80 – 90% amorphous silica, 1 – 2% potassium oxide (K₂O) and the rest is carbon (Jamo and Maharaz, 2015). The substantial silica content of rice husk ash has excellent potential as a source of silica (Na₂SiO₃)_(RHA) for the production of new material-based silica (Hastuti *et al.*, 2020, 2019; Sakti *et al.*, 2013). Furthermore, silica has the advantage of good

Cite this as: Hastuti, S., Martini, T., Wibowo, A. H., Fitriana, D., Zuhara, W., Mutma'inah, H., and Putri, R. I., 2025. Removal of Heavy Metals: Pb(II), Ni(II), and Cd(II) by Fe₃O₄@SiO₂-TMPDT Adsorbent Prepared from Rice Husk Ash. *ALCHEMY Jurnal Penelitian Kimia*, 21(1), 53-63. <https://dx.doi.org/10.20961/alchemy.21.1.91934.53-63>.

thermal and mechanical stability, large surface area, stability in acids, and good surface modification properties (Fahmiati *et al.*, 2018). The silica surface contains silanol (Si–OH), which is easily modified with functional groups such as amine (Kheshti *et al.*, 2019; Liu *et al.*, 2016; Robles-Jimarez *et al.*, 2022), carboxylic (Jabbari-Gargari *et al.*, 2021; Jiaqi *et al.*, 2019), and thiols (Beagan *et al.*, 2022; Sharma *et al.*, 2022).

The magnetic properties of the adsorbent are advantageous because they easily separate from the solution using an external magnetic field. Several studies on adsorption using silica with magnetic properties have been carried out (Fahmiati *et al.*, 2018; Javaheri *et al.*, 2019; Kheshti *et al.*, 2019; Wang *et al.*, 2010), such as the synthesis of functionalized magnetized silica 3-Aminopropyl triethoxysilane (APTES) for adsorption of nitrate ions (Kheshti *et al.*, 2019), synthesis of magnetized silica modified by L-Arginine (Amaria *et al.*, 2017), functionalized magnetized silica with 3-Aminopropyl trimethoxysilane (APTMS) (Tang *et al.*, 2013), with 3-Aminopropyl triethoxysilane (APTES) (Javaheri *et al.*, 2019; Saadat *et al.*, 2019) and diethylenetriamine (Fahmiati *et al.*, 2018). In this study, efforts were made to increase the ability of silica as an adsorbent by adding Fe₃O₄ to Na₂SiO_{3(RHA)}. Furthermore, the result is then modified with N³-(3-trimethoxysilylpropyl) diethylenetriamine (TMPDT) to form Fe₃O₄@SiO₂-TMPDT, with three amine groups which will increase the adsorption capacity. The adsorption process of Fe₃O₄@SiO₂-TMPDT, including the variations in pH, adsorption contact time, and ion concentrations of Pb(II), Ni(II), and Cd(II), was also examined.

RESEARCH METHODS

Equipment and Materials

The equipment used were a 200-mesh sieve, hot plate, filter paper, analytical balance, oven, pH meter, shaker, sonicator, furnace, Fourier Transform Infra-Red spectrophotometer (FTIR), Shimadzu type IR Prestige-21, and Atomic Absorption Spectrometer (AAS), Shimadzu type AA-6650F). The materials used were distilled water, sodium hydroxide, hydrochloric acid, iron oxide Fe₃O₄, and salts of Pb(NO₃), Ni(NO₃), and Cd(NO₃) that were purchased from Merck. N³-(3-trimethoxysilylpropyl) diethylenetriamine (TMPDT) was purchased from Sigma-Aldrich.

Experiment

The process of preparing sodium silicate involves mixing 10 g of rice husk ash (200 mesh) with 80 mL of 4M NaOH, heating to 100 °C, and stirring until thick. It was further heated at 500 for 30 minutes, and after cooling, 100 mL distilled water was added, resulting in a filtrate of sodium silicate Na₂SiO_{3(RHA)}. (Sakti *et al.*, 2013). The synthesis of Fe₃O₄@SiO₂-TMPDT refers to previous studies with some modifications (Amaria *et al.*, 2017). The adsorbent was prepared with varying compositions of suspension Fe₃O₄, namely Na₂SiO_{3(RHA)} (v/v) 1:4, 2:3, and 1:1, and then 1 mL TMPDT was added. The composition of 1:4 (v/v) was carried out by adding 5 mL distilled water to 0.2 g Fe₃O₄ sonicated for 5 minutes, and 20 mL Na₂SiO_{3(RHA)} was added and sonicated for 15 minutes. Next, 1 mL of TMPDT was added to the resulting solution, stirred for 1 hour, and 6 M HCl was gradually added to form a gel. The gel was dried at 70 °C for 18 hours, washed with ethanol-aquadest (1:1), and dried at 70 °C for 5 hours. Applying the same treatment in the ratio 2:3 (v/v), wherein 0.4 g Fe₃O₄ was added into 10 mL distilled water and 15 mL Na₂SiO_{3(RHA)}, while the ratio 1:1 (v/v) involved the addition of 0.5 g Fe₃O₄ into a 12.5 mL distilled water and 12.5 mL Na₂SiO_{3(RHA)}. The TMPDT variations are carried out by adding 1 mL, 2.5 mL, and 5 mL.

pH Optimization

An amount of 10 mg of Fe₃O₄@SiO₂-TMPDT adsorbent was added to 10 mL of a 10 ppm solution of Pb(II), Ni(II), and Cd(II) metal ions. The adsorption process was carried out at different pH levels 3, 4, 5, and 6 to investigate the effect of pH on the adsorption efficiency for each metal ion.

Adsorption Kinetic Studies

An amount of 10 mg of Fe₃O₄@SiO₂-TMPDT adsorbent was introduced into 10 mL of a 10 ppm solution of Pb(II), Ni(II), and Cd(II) metal ions, and the adsorption process was conducted over varying contact times of 10, 20, 40, 70, 100, and 120 minutes at the optimum pH. The data collected from these experiments were utilized to analyze the adsorption kinetics by fitting the results to various kinetic models, including first-order (Equation (1)), second-order (Equation (2)), pseudo-first-order (Equation (3)), and pseudo-second-order (Equation (4)) models.

$$\ln C_e = -kt + \ln C_0 \quad (1)$$

$$\frac{1}{C_0} = \frac{1}{C_e} + kt \quad (2)$$

$$\ln (q_e - q_t) = \ln q_e - kt \quad (3)$$

$$\frac{t}{q_t} = \frac{1}{k_2 q_e^2} + \frac{t}{q_e} \quad (4)$$

Where C_0 = concentration (metal ions) at $t = 0$ (ppm), C_e = concentration (metal ions) at $t = t$ (ppm), k = reaction rate constant, t = time (minutes), q_e = equilibrium adsorption capacity (mg/g), q_t = adsorption capacity at a specific time t (mg/g).

Adsorption Isotherm Studies

A total of 10 mg of $\text{Fe}_3\text{O}_4@\text{SiO}_2\text{-TMPDT}$ 10 was contacted with 10 mL metal ions with concentrations of 2, 4, 6, 8, 10, and 12 ppm at optimum pH. The collected data were applied to study the Langmuir isotherm (Equation (5)) and Freundlich isotherm (Equation (6)) models.

$$\frac{C_e}{q_e} = \frac{1}{q_m} C_e + \frac{1}{K_L q_m} \quad (5)$$

$$\ln q_e = \ln K_f - \frac{1}{n} \ln C_e \quad (6)$$

Where C_e = metal ion concentration in solution after adsorption (mg/L), q_m = maximum adsorption capacity (mg/g), K_L = Langmuir constant (L/mg), = Freundlich's constant related to adsorption intensity, K_f = Freundlich constant concerning adsorption capacity.

RESULTS AND DISCUSSION

Adsorbent $\text{Fe}_3\text{O}_4 @ \text{SiO}_2\text{-TMPDT}$

The optimization of the suspension $\text{Fe}_3\text{O}_4:\text{Na}_2\text{SiO}_3(\text{RHA})$ (v/v) composition is presented in Table 1. It was observed that at a 1:4 ratio, the adsorbent had the highest weight, followed by the 2:3 and 1:1 ratios. This trend can be attributed to the fact that a higher proportion of $\text{Na}_2\text{SiO}_3(\text{RHA})$ leads to the formation of a denser and more solid silica gel. A well-balanced composition is essential to ensure that the resulting gel is solid and easily separable using a magnet due to the magnetic properties imparted by the Fe_3O_4 . Among the different ratios tested, the 2:3 ratio was found to be the most optimal for the synthesis of adsorbents. This particular composition resulted in a material with strong magnetic characteristics, making it efficient for applications requiring magnetic separation. The balance between Fe_3O_4 and $\text{Na}_2\text{SiO}_3(\text{RHA})$ in the 2:3 ratio provided a solid gel structure that was both magnetically responsive and mechanically stable, making it suitable for further adsorption experiments.

Table 1. The mass and the magnetic strength of $\text{Fe}_3\text{O}_4:\text{Na}_2\text{SiO}_3$ in various composition ratios.

$\text{Fe}_3\text{O}_4:\text{Na}_2\text{SiO}_3$ (v/v)	Adsorbent mass (g)	Magnetic Power
1:4	5.99	Weak
2:3	4.57	Good
1:1	4.16	Good

The optimization of the TMPDT volume is illustrated in Figure 1. It was observed that increasing the amount of TMPDT made the gel formation process more difficult. This is due to the increased condensation, which disrupts the formation of siloxane bonds within the silica structure. As a result, the stability of the gel network is compromised, making it less robust. In this study, 1 mL of TMPDT was determined to be the optimal amount. This volume provided a balance between achieving sufficient functionalization of the silica surface while maintaining the structural stability of the gel, allowing for effective synthesis without significant disruption to the siloxane bond formation.



Figure 1. $\text{Fe}_3\text{O}_4@SiO_2$ -TMPDT with (a) 1 mL TMPDT variation, (b) 2.5 mL, and (c) 5 mL.

The possible reaction mechanism for forming $\text{Fe}_3\text{O}_4@SiO_2$ -TMPDT is shown in Figure 2. Sodium silicate ($\text{Na}_2\text{SiO}_3(\text{RHA})$) (I) is initially added to hydrochloric acid (HCl), leading to the formation of tetrahydrosilicate $\text{Si}(\text{OH})_4$ (II) and sodium chloride (NaCl) as a byproduct. In the next step, $\text{Si}(\text{OH})_4$ reacts with Fe_3O_4 to form $\text{Fe}_3\text{O}_4@SiO_2$ (III), where the silica shell coats the magnetic Fe_3O_4 core. The presence of hydroxyl ($-\text{OH}$) groups on the surface of $\text{Fe}_3\text{O}_4@SiO_2$ provides active silanol sites that facilitate further reactions. These silanol groups then react with $N^-(3\text{-trimethoxysilylpropyl})$ diethylenetriamine (TMPDT) (IV), a silane coupling agent, to form the final product, $\text{Fe}_3\text{O}_4@SiO_2$ -TMPDT (V). In this final structure, TMPDT functionalizes the silica-coated magnetic, introducing amine functional groups that are crucial for enhancing adsorption properties and providing specific binding sites for metal ions.

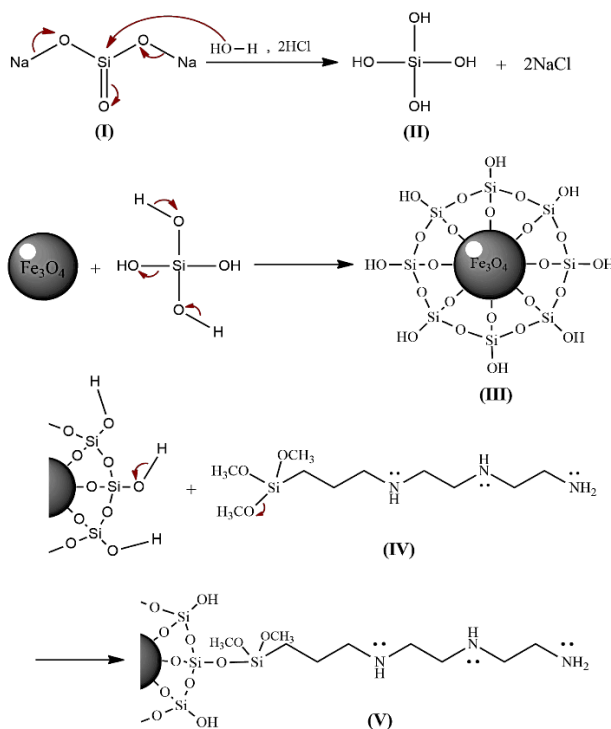


Figure 2. Mechanism reaction of $\text{Fe}_3\text{O}_4@SiO_2$ -TMPDT.

Functional Groups Characteristics of $\text{Fe}_3\text{O}_4@SiO_2$ -TMPDT

The functional groups of the prepared material were analyzed from FTIR spectra, as presented in Figure 3. For SiO_2 (a), the characteristic peaks corresponding to the siloxane groups ($\text{Si}-\text{O}-\text{Si}$) were observed at 1075 cm^{-1} , and the silanol groups ($\text{Si}-\text{OH}$) were identified at 795 cm^{-1} , which are the primary functional groups of SiO_2 . Additionally, the bending and stretching vibrations of water (H_2O) molecules were detected at 1642 cm^{-1} and 3456 cm^{-1} , respectively, representing the presence of moisture in the sample. In contrast, the spectrum of Fe_3O_4 (b) exhibited a distinct and sharp absorption band at 570 cm^{-1} with high intensity, characteristic of the $\text{Fe}-\text{O}$ stretching vibration, which is indicative of the magnetite phase. Upon coating Fe_3O_4 with SiO_2 , forming $\text{Fe}_3\text{O}_4@SiO_2$ (c), the FTIR spectrum revealed several key peaks, including $\text{Si}-\text{O}$ at 795 cm^{-1} , $\text{Si}-\text{O}-\text{Si}$ at 1082 cm^{-1} , $\text{O}-\text{H}$ bending

at 1643 cm^{-1} , O–H stretching at 3452 cm^{-1} , and the Fe–O stretching at 567 cm^{-1} , confirming the successful synthesis of the $\text{Fe}_3\text{O}_4@\text{SiO}_2$.

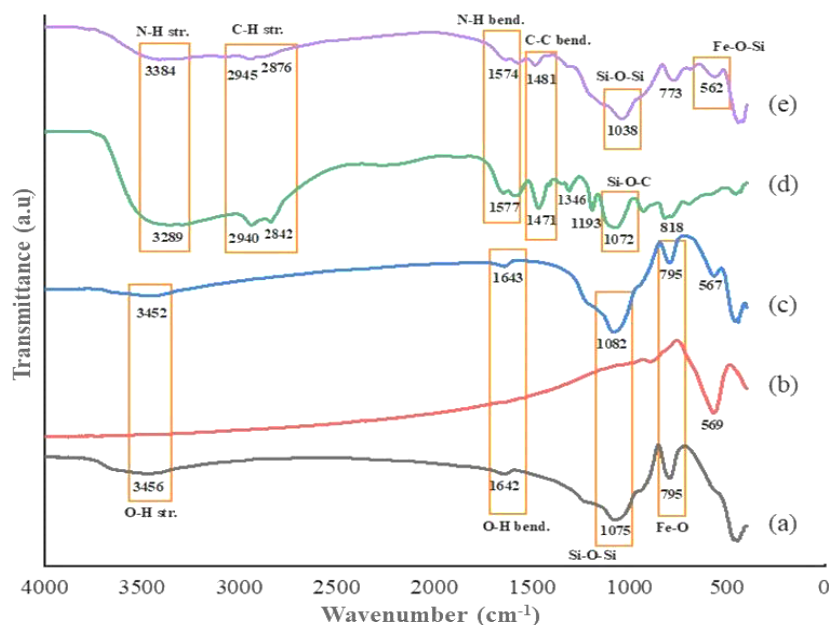


Figure 3. FTIR spectra of (a) SiO_2 , (b) Fe_3O_4 , (c) $\text{Fe}_3\text{O}_4@\text{SiO}_2$, (d) TMPDT, and (e) $\text{Fe}_3\text{O}_4@\text{SiO}_2$ -TMPDT.

TMPDT (d) was identified by characteristic peaks at 1072 cm^{-1} , 1346 cm^{-1} , and 1471 cm^{-1} , which correspond to C–C stretching, C–H bending, and C–C bending vibrations, respectively. The C–H stretching vibrations of methyl ($-\text{CH}_3$) and methylene ($-\text{CH}_2-$) groups were observed at 2940 cm^{-1} and 2842 cm^{-1} , respectively. Furthermore, the amine functional groups were detected through N–H bending at 1577 cm^{-1} and N–H stretching at 3289 cm^{-1} . For $\text{Fe}_3\text{O}_4@\text{SiO}_2$ -TMPDT (e), specific vibrational peaks were observed at 562 cm^{-1} for Fe–O–Si, 1038 cm^{-1} for Si–O–Si, 1574 cm^{-1} for N–H bending, and 3384 cm^{-1} for N–H stretching, confirming the presence of siloxane and amine groups on the functionalized surface. Additionally, the C–H stretching vibrations of $-\text{CH}_3$ and $-\text{CH}_2-$ groups were identified at 2945 cm^{-1} and 2876 cm^{-1} , respectively, further confirming the successful functionalization of the material with organic groups.

The pH Optimization

Adjusting the pH of the solution directly influences the concentration of H^+ and OH^- ions in the system. Under acidic conditions, an excess of H^+ ions competes with metal ions to bind to the amine group ($-\text{NH}_2$) on the surface of the adsorbent. Given that H^+ ions act as stronger Lewis acids compared to metal ions (Rahayu and Khabibi, 2016), their presence significantly reduces the chance of metal ions interacting with the active sites on the adsorbent. As a result, the adsorbent's capacity for metal ion adsorption is reduced. Furthermore, the high concentration of H^+ ions in acidic solutions causes the amine groups to become protonated, leading to electrostatic repulsion between the positively charged adsorbent surface and the metal ions, further decreasing adsorption efficiency, as depicted in Figure 4.

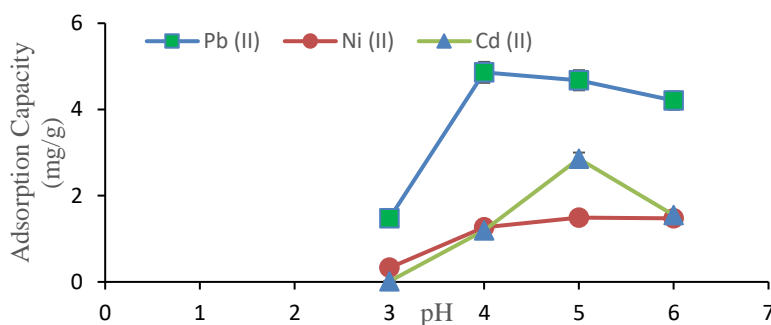


Figure 4. Impact of solution pH on adsorption capacity.

On the other hand, in highly alkaline conditions, the concentration of OH^- ions increases. These hydroxyl ions can react with metal ions to form metal hydroxide precipitates, thereby reducing the concentration of free metal ions in the solution. This process ultimately limits the interaction between the amine groups ($-\text{NH}_2$) on the adsorbent and the metal ions, further decreasing the total adsorption capacity. Figure 4 illustrates that the adsorption of metal ions increases as the pH approaches the optimum level, which is attributed to the reduction in H^+ ion concentration in the solution, allowing more metal ions to bind to the active sites on the adsorbent. However, at pH values higher than the optimum, adsorption capacity decreases due to the increasing concentration of OH^- ions in the solution, which interact with metal ions to form metal hydroxide precipitates, reducing the availability of free metal ions for adsorption. In this study, the optimum pH for Pb(II) and Ni(II) was found to be 4, whereas for Cd(II), it was 5.

Adsorption Kinetic Study

The variation in contact time was used to determine the equilibrium time during the adsorption process between the metal ions and the $\text{Fe}_3\text{O}_4@\text{SiO}_2\text{-TMPDT}$ adsorbent. The determination of contact time variation was conducted at the optimum pH for the respective ions, Pb(II), Ni(II), and Cd(II). Figure 5 illustrates the relationship between contact time and adsorption capacity, showing how the adsorption capacity changes as a function of time.

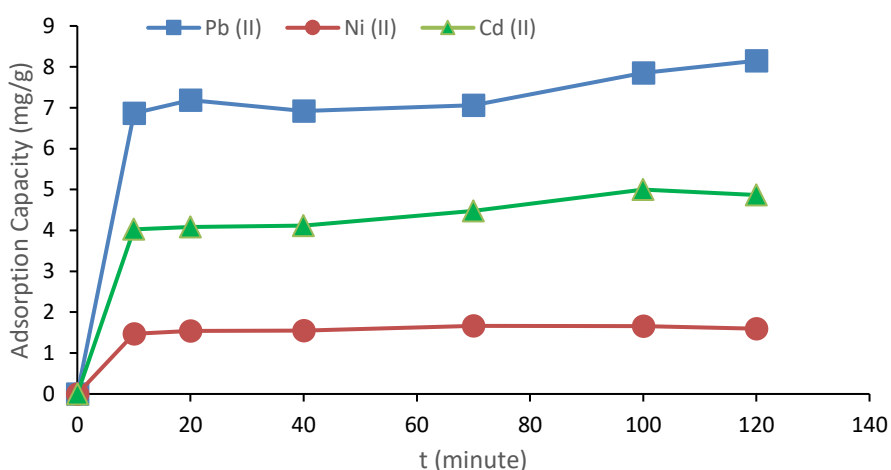


Figure 5. Variation of contact time versus adsorption capacity.

Figure 5 shows that equilibrium initiation has occurred at a contact time of 10 minutes. As the contact time increases, its effect on enhancing adsorption capacity diminishes, and equilibrium is achieved quickly. This shows that the pore effect of the adsorbent on the adsorption process is small, and it is more influenced by the interaction of the active sites on the adsorbent than the pores. Furthermore, the adsorption kinetic model was determined based on first-order (Equation (1)), second-order (Equation (2)), pseudo-first-order (Equation (3)), and pseudo-second-order (Equation (4)). The first-order kinetic is obtained by plotting the contact time (t) against $\ln C_e$, while the contact time (t) was plotted against $1/C_e$ for the second-order. For pseudo-first-order kinetic, the model was determined by plotting the contact time against $\ln(q_e - qt)$ while the contact time was plotted against t/qt for the pseudo-second-order.

Table 2 shows the adsorption kinetic model on $\text{Fe}_3\text{O}_4@\text{SiO}_2\text{-TMPDT}$ for Pb(II), Ni(II), and Cd(II) ions following pseudo-second-order. This is evidenced by the value of R^2 for each metal ion, which is close to the value of 1, which is a pseudo-second-order kinetic model. The kinetic model indicated that the interaction between the adsorbent and adsorbate is chemical in nature. This is dominated by interactions through active sites rather than pores, supported by the relatively short equilibrium time of 10 minutes. Adsorption tends to occur chemically when the calculated value is close to the experimental value (Hastuti *et al.*, 2015). Table 3 shows that the calculated q_e value ($q_{e \text{ cal}}$) closely approximates the experimental q_e ($q_{e \text{ exp}}$) value within the pseudo-second-order. In contrast, a significant disparity is observed within the first-order pseudo-kinetic model. The value of $q_{e \text{ cal}}$ in the pseudo-first and second order is determined by plotting the data in Equations 3 and 4, while the $q_{e \text{ exp}}$ is obtained from experimental data.

Table 2. Kinetic parameters of various metal ions.

Kinetic Models	Kinetic parameters					
	Pb(II)		Ni(II)		Cd(II)	
	R ²	K	R ²	k	R ²	K
first-order	0.783	0.00020	0.7629	0.00020	0.9231	-0.0020
second-order	0.782	0.00003	0.7640	0.00003	0.9296	-0.0005
pseudo-first-order	0.023	-0.0333	0.9884	-0.0333	0.9742	0.0018
pseudo-second-order	0.992	8140.6	0.9996	8140.6	0.9945	0.0339

Table 3. Value of q_e results of calculations and experiments for several metal ions.

Metal	q_e cal		q_e exp
	Pseudo-first-order	Pseudo-second-order	
Pb(II)	4.15×10^{-6}	3.8×10^{-5}	3.96×10^{-5}
Ni(II)	3.8×10^{16}	1.23×10^{-4}	1.27×10^{-4}
Cd(II)	1.2749	5.0994	4.9984

Adsorption Isotherm Study

The Langmuir isotherm shows a chemical interaction occurs between the adsorbent and the adsorbate. The interaction of metal ions on the adsorbent forms a monolayer, and the adsorption on each side is homogeneous (Wijayanti and Kurniawati, 2019). Furthermore, the Freundlich isotherm showed a physical interaction of the adsorbent with metal ions. The physical interaction forms a multilayer, and the adsorbent sides are heterogeneous, resulting in different energy bonds on each side (Wijayanti and Kurniawati, 2019). The interaction between metal ions and adsorbents can occur through van der Waals forces or pores. Van der Waals forces arise due to dipole-dipole between the surface of the adsorbent and the metal ion. Equations 5 and 6 were used to calculate adsorption capacity (q_m), Langmuir constant (k_L), Freundlich adsorption capacity (k_f), and intensity (n). Table 4 shows that the adsorption process for Pb(II), Ni(II), and Cd(II) ions follows the Langmuir isotherm model with the R^2 value closest to 1.

Table 4. Isotherm adsorption parameter on $Fe_3O_4@SiO_2$ -TMPDT adsorbent.

Isotherm adsorption	Parameter	Pb(II)	Ni(II)	Cd(II)
Langmuir	R^2	0.9770	0.9862	0.9973
	q_m (mg/g)	11.760	1.864	1.88 8
	k_L (L/mg)	0.699	0.577	9.546
Freundlich	R^2	0.930	0.936	0.674
	k_f (mg/g)	5.320	0.116	1.46 8

These findings suggest a chemical interaction between the adsorbent and metal ions at the active site (amine group) on the surface of $Fe_3O_4@SiO_2$ -TMPDT rather than within the pores, as depicted in Figure 6. Figure 6 illustrates the binding of Pb(II), Ni(II), and Cd(II) metal ions to the $Fe_3O_4@SiO_2$ -TMPDT adsorbent through chemisorption. This process occurs at the active sites (amine groups) on the surface of $Fe_3O_4@SiO_2$ -TMPDT. The amine groups from TMPDT contain lone pair electrons, which bind to the positively charged metal ions (M^{2+}). In addition, the binding of metal ions (M^{2+}) can also occur through the lone pair electrons of siloxane and silanol groups on the silica surface, forming weak chemical bonds. Meanwhile, physisorption interactions may take place between metal ions (M^{2+}) and the pores in silica. Physisorption allows the adsorption of metal ions to form a multilayer, where adsorption within the silica pores continues until the pores are completely filled with the adsorbate, reaching the maximum adsorption capacity.

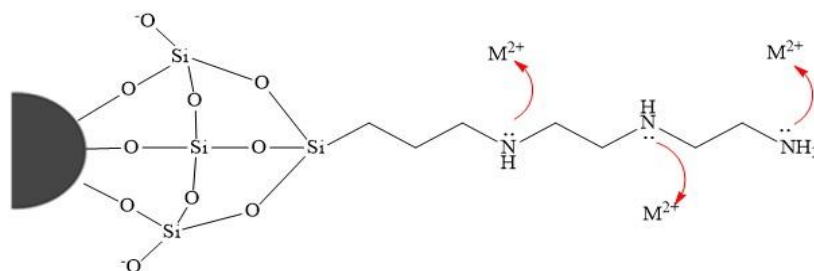


Figure 6. Binding mechanism of metal ions by $\text{Fe}_3\text{O}_4@\text{SiO}_2\text{-TMPDT}$.

Table 5 presents the maximum adsorption capacity (q_m) values for various adsorbents and adsorbates. The value of the maximum adsorption capacity (q_m) for $\text{Pb(II)} > \text{Cd(II)} > \text{Ni(II)}$ was 11.760, 1,888, and 1,864 mg/g, respectively. The electron configuration of Pb, Cd, and Ni atoms are 6, 5, and 4 electron shells, respectively. Furthermore, a more significant number of electron shells results in a larger atom size, causing the atomic nucleus's attraction to weaken. This phenomenon facilitates the release of outer electrons, leading to the formation of cations.

Table 5. Comparison of maximum adsorption capacity of other adsorbents with $\text{Fe}_3\text{O}_4@\text{SiO}_2\text{-TMPDT}$.

Material	Adsorbate	Adsorption capacity q_m (mg/g)	Reference
$\text{Fe}_3\text{O}_4@\text{SiO}_2\text{-TMPDT}$	Pb(II)	11.760	Present work
$\text{Fe}_3\text{O}_4@\text{SiO}_2\text{-TMPDT}$	Ni(II)	1.864	Present work
$\text{Fe}_3\text{O}_4@\text{SiO}_2\text{-TMPDT}$	Pb(II)	1.888	Present work
<i>Polyaniline/silica gel</i> (PANI/ SiO_2)	Cd(II)	51.02	(Putrinesia <i>et al.</i> , 2019)
<i>silica@mercapto</i> (HS@M)	Pb(II)	4.97	(Naat <i>et al.</i> , 2021)
Rise husk	Cd(II)	5.13	(Montalvo-Andía <i>et al.</i> , 2022)
Silica-based sandwich-layered zirconium-titanium phosphate	Ni(II)	50.01	(Li <i>et al.</i> , 2021)
Silica-chitosan beads	Ni(II)	40.32	(Sertsing <i>et al.</i> , 2018)
EDTA modified silica airgel	Ni(II)	84.75	(Pornchuti <i>et al.</i> , 2020)

Based on Table 5, the $\text{Fe}_3\text{O}_4@\text{SiO}_2\text{-TMPDT}$ adsorbent demonstrates a lower adsorption capacity compared to others. This is due to the fact that Fe_3O_4 is not an adsorbent with pores as effective as silica. Therefore, the addition of Fe_3O_4 tends to reduce its adsorption ability. Nevertheless, $\text{Fe}_3\text{O}_4@\text{SiO}_2\text{-TMPDT}$ offers advantages, such as ease of separation from the solution by simply bringing a magnet close to the adsorbent. This feature is highly beneficial in water purification filtration applications to remove heavy metal contaminants.

CONCLUSION

In conclusion, $\text{Fe}_3\text{O}_4@\text{SiO}_2\text{-TMPDT}$ adsorbent was successfully synthesized using the sol-gel method, combining sodium silicate derived from rice husk ash ($\text{Na}_2\text{SiO}_3(\text{RHA})$), magnetite (Fe_3O_4), and TMPDT. The FTIR spectra of $\text{Fe}_3\text{O}_4@\text{SiO}_2\text{-TMPDT}$ confirmed the formation of new functional groups, including Fe-O-Si, amine, and C-H groups from the TMPDT. Furthermore, the optimal pH for the adsorption of metal ions was determined to be 4 for Pb(II) and Ni(II) and 5 for Cd(II). The adsorption kinetics of Pb(II), Ni(II), and Cd(II) onto $\text{Fe}_3\text{O}_4@\text{SiO}_2\text{-TMPDT}$ followed the pseudo-second-order kinetic model, while the adsorption isotherm aligned with the Langmuir model. The maximum adsorption capacities were found to be 11.760 mg/g for Pb(II), 1.864 mg/g for Ni(II), and 1.888 mg/g for Cd(II). These findings suggest that $\text{Fe}_3\text{O}_4@\text{SiO}_2\text{-TMPDT}$ is a promising material for the effective removal of heavy metal ions, such as Pb(II), Ni(II), and Cd(II), from aqueous solutions.

CONFLICT OF INTEREST

There is no conflict of interest in this article.

AUTHOR CONTRIBUTION

SH: Conceptualization, Resources, Methodology, Supervision, Manuscript Review, Manuscript Revision; TM: Supervision; AHW: Editing; DF: Editing; WZ: Data Analysis, Manuscript Drafting; HM: Data Analysis, Manuscript Drafting; RIP: Data Analysis, Manuscript Drafting.

ACKNOWLEDGMENT

The authors would like to thank Sebelas Maret University for providing HRG grant No 228/UN27.22/PT.01.03/2023.

REFERENCES

- Amaria, Suyanta, and Nuryono, 2017. Coating of L-Arginine Modified Silica on Magnetite through Two Different Sol-Gel Routes. *Indonesian Journal of Chemical*, 17, 256–263. <https://doi.org/10.22146/ijc.23642>.
- Awual, M.R., Hasan, M.M., and Shahat, A., 2014. Functionalized Novel Mesoporous Adsorbent for Selective Lead(II) Ions Monitoring and Removal from Wastewater. *Sensors and Actuators, B: Chemical*, 203, 854–863. <https://doi.org/10.1016/j.snb.2014.07.063>.
- Azimi, A., Azari, A., Rezakazemi, M., and Ansarpour, M., 2017. Removal of Heavy Metals from Industrial Wastewaters: A Review. *ChemBioEng Reviews*, 4, 37–59. <https://doi.org/10.1002/cben.201600010>.
- Beagan, A., Alotaibi, K., Almakhlafi, M., Algarabli, W., Alajmi, N., Alanazi, M., Alwaalah, H., Alharbi, F., Alshammari, R., and Alswieleh, A., 2022. Amine and Sulfonic Acid Functionalized Mesoporous Silica As An Effective Adsorbent for Removal of Methylene Blue from Contaminated Water. *Journal of King Saud University - Science*, 34, 101762. <https://doi.org/10.1016/j.jksus.2021.101762>.
- Bheel, N., Meghwar, S.L., Abbasi, S.A., Marwari, L.C., Muger, J.A., and Abbasi, R.A., 2018. Effect of Rice Husk Ash and Water-Cement Ratio on Strength of Concrete. *Civil Engineering Journal*, 4, 2373. <https://doi.org/10.28991/cej-03091166>.
- Dong, Z., Zhang, F., Wang, D., Liu, X., and Jin, J., 2015. Polydopamine-Mediated Surface-Functionalization of Graphene Oxide for Heavy Metal Ions Removal. *Journal of Solid State Chemistry*, 224, 88–93. <https://doi.org/10.1016/j.jssc.2014.06.030>.
- Fahmiati, Nuryono, and Suyanta, 2018. Functionalization of Silica Coated on Iron Sand Magnetic Material with Diethylenetriamine. *Asian Journal of Chemistry*, 30, 1805–1810. <https://doi.org/10.14233/ajchem.2018.21314>.
- Hajiaghababaei, L., Badii, A., Ganjali, M.R., Heydari, S., Khaniani, Y., and Ziarani, G.M., 2011. Highly Efficient Removal and Preconcentration of Lead and Cadmium Cations from Water and Wastewater Samples Using Ethylenediamine Functionalized SBA-15. *Desalination*, 266, 182–187. <https://doi.org/10.1016/j.desal.2010.08.024>.
- Hastuti, S., Nuryono, and Kuncaka, A., 2019. Synthesis and Characterization of L-Arginine Modified Silica by Sol-Gel Method Prepared Rice Hull Ash. *IOP Conference Series: Materials Science and Engineering*, 509. <https://doi.org/10.1088/1757-899X/509/1/012135>.
- Hastuti, S., Nuryono, and Kuncaka, A., 2015. L-Arginine-Modified Silica for Adsorption of Gold(III). *Indonesian Journal of Chemistry*, 15, 108–115. <https://doi.org/10.22146/ijc.21203>.
- Hastuti, S., Wahyuningsih, S., Martini, T., Fajariani, E.N., and Candraningrum, I.K., 2020. Synthesis of N'-(3-Trimethoxysilylpropyl) Diethylenetriamine Modified Silica (SiO₂(RHA)-TMPDT) for Adsorption of Gold (III). in *AIP Conference Proceedings*, 2237.
- Huang, Y., Zeng, X., Guo, L., Lan, J., Zhang, L., and Cao, D., 2018. Heavy Metal Ion Removal of Wastewater by Zeolite-Imidazolate Frameworks. *Separation and Purification Technology*, 194, 462–469. <https://doi.org/10.1016/j.seppur.2017.11.068>.
- Jabbari-Gargari, A., Moghaddas, J., Hamishehkar, H., and Jafarizadeh-Malmiri, H., 2021. Carboxylic Acid Decorated Silica Aerogel Nanostructure As Drug Delivery Carrier. *Microporous and Mesoporous Materials*, 323, 111220. <https://doi.org/10.1016/j.micromeso.2021.111220>.
- Jamo, U.H., and Maharaz, M.N., 2015. Influence of Addition of Rice Husk Ash on Porcelain Composition. *Science World Journal*, 10, 7–16.
- Javaheri, F., Kheshti, Z., Ghasemi, S., and Altaee, A., 2019. Enhancement of Cd²⁺ Removal from Aqueous Solution by Multifunctional Mesoporous Silica: Equilibrium Isotherms and Kinetics Study. *Separation and Purification Technology*, 224, 199–208. <https://doi.org/10.1016/j.seppur.2019.05.017>.

- Jiaqi, Z., Yimin, D., Danyang, L., Shengyun, W., Liling, Z., and Yi, Z., 2019. Synthesis of Carboxyl-Functionalized Magnetic Nanoparticle for The Removal of Methylene Blue. *Colloids and Surfaces A: Physicochemical and Engineering Aspects*, 572, 58–66. <https://doi.org/10.1016/j.colsurfa.2019.03.095>.
- Kheshti, Z., Ghajar Azodi, K., Altaee, A., and Kheshti, M.R., 2019. High-Gradient Magnetic Separator (HGMS) Combined with Adsorption for Nitrate Removal from Aqueous Solution. *Separation and Purification Technology*, 212, 650–659. <https://doi.org/10.1016/j.seppur.2018.11.080>.
- Li, C., Zhao, J., and Zhang, Y., 2021. Study on Adsorption Behavior of Nickel Ions Using Silica-Based Sandwich Layered Zirconium-Titanium Phosphate Prepared by Layer-By-Layer Grafting Method. *Nanomaterials*, 11. <https://doi.org/10.3390/nano11092314>.
- Liu, Y., Fu, R., Sun, Y., Zhou, X., Baig, S.A., and Xu, X., 2016. Multifunctional Nanocomposites Fe₃O₄@SiO₂-EDTA for Pb(II) and Cu(II) Removal from Aqueous Solutions. *Applied Surface Science*, 369, 267–276. <https://doi.org/10.1016/j.apsusc.2016.02.043>.
- Minister of Health Regulation Number 2, 2023. Kementerian Kesehatan Republik Indonesia. Jakarta.
- Montalvo-Andía, J., Reátegui-Romero, W., Peña-Contreras, A.D., Zaldivar Alvarez, W.F., King-Santos, M.E., Fernández-Guzmán, V., Guerrero-Guevara, J.L., and Puris-Naupay, J.E., 2022. Adsorption of Cd (II) Using Chemically Modified Rice Husk: Characterization, Equilibrium, and Kinetic Studies. *Adsorption Science and Technology*, 2022, 17. <https://doi.org/10.1155/2022/3688155>.
- Naat, J.N., Neolaka, Y.A.B., Lapailaka, T., Tj, R.T., Sabarudin, A., Darmokoesoemo, H., and Kusuma, H.S., 2021. Adsorption of Cu(II) and Pb(II) Using Silica@mercpto (Hs@m) Hybrid Adsorbent Synthesized from Silica of Takari Sand: Optimization of Parameters and Kinetics. *Rasayan Journal of Chemistry*, 14, 550–560. <https://doi.org/10.31788/RJC.2021.1415803>.
- Namasivayam, C., and Ranganathan, K., 1995. Removal of Pb(Ii), Cd(Ii), Ni(Ii) and Mixture of Metal Ions by Adsorption onto 'waste' Fe(Iii)/Cr(Iu) Hydroxide and Fixed Bed Studies. *Environmental Technology (United Kingdom)*, 16, 851–860. <https://doi.org/10.1080/09593330.1995.9618282>.
- Pornchuti, B., Pongpattananurak, B., Sutthiard, D., and Singthong, P., 2020. Adsorption of Copper, Nickel and Chromium Ions Using Silica Aerogel Synthesized by Ambient-Pressure Drying and Modified with EDTA. *IOP Conference Series: Materials Science and Engineering*, 778. <https://doi.org/10.1088/1757-899X/778/1/012133>.
- Putrinesia, M.I., Nurlina, N., and Rahmalia, W., 2019. Adsorption of Pb(II) by Polyaniline/Silica Gel Composite: Kinetics and Isotherm Studies. *Indonesian Journal of Pure and Applied Chemistry*, 1, 91. <https://doi.org/10.26418/indonesian.v1i3.34196>.
- Rahayu, P., and Khabibi, 2016. Adsorpsi Ion Logam Nikel(II) Oleh Kitosan Termodifikasi Tripolifosfat. *Jurnal Kimia Sains dan Aplikasi*, 19, 21–26. <https://doi.org/10.14710/jksa.19.1.21-26>.
- Robles-Jimarez, H.R., Sanjuan-Navarro, L., Jornet-Martínez, N., Primaz, C.T., Teruel-Juanes, R., Molins-Legua, C., Ribes-Greus, A., and Campíns-Falcó, P., 2022. New Silica Based Adsorbent Material from Rice Straw and Its In-Flow Application to Nitrate Reduction in Waters: Process Sustainability and Scale-Up Possibilities. *Science of the Total Environment*, 805, 50317. <https://doi.org/10.1016/j.scitotenv.2021.150317>.
- Saadat, A., Hajiaghababaei, L., Badiei, A., Ganjali, M.R., and Mohammadi Ziarani, G., 2019. Amino Functionalized Silica Coated Fe₃O₄ Magnetic Nanoparticles as a Novel Adsorbent for Removal of Pb²⁺ and Cd²⁺. *Pollution*, 5, 847–857. <https://doi.org/10.22059/poll.2019.274986.573>.
- Sakti, S.C.W., Siswanta, D., and Nuryono, 2013. Adsorption of Gold(III) on Ionic Imprinted Amino-Silica Hybrid Prepared from Rice Hull Ash. *Pure and Applied Chemistry*, 85, 211–223. <https://doi.org/10.1351/PAC-CON-12-01-02>.
- Sertsing, S., Chukeaw, T., Pengpanich, S., and Pornchuti, B., 2018. Adsorption of Nickel and Chromium Ions by Amine-Functionalized Silica Aerogel. *MATEC Web of Conferences*, 156, 4–7. <https://doi.org/10.1051/mateconf/201815603014>.
- Sharma, S., Walia Kumar, Y., Grover, G., and Sanjeev, V.K., 2022. Effect of Surface Modification of Silica Nanoparticles with Thiol Group on the Shear Thickening Behaviors of the Suspensions of Silica Nanoparticles in Polyethylene Glycol (PEG). *IOP Conference Series: Materials Science and Engineering*, 1225, 012053. <https://doi.org/10.1088/1757-899x/1225/1/012053>.
- Tang, Y., Liang, S., Wang, J., Yu, S., and Wang, Y., 2013. Amino-Functionalized Core-Shell Magnetic Mesoporous Composite Microspheres for Pb(II) and Cd(II) Removal. *Journal of Environmental Sciences (China)*, 25, 830–837. [https://doi.org/10.1016/S1001-0742\(12\)60141-7](https://doi.org/10.1016/S1001-0742(12)60141-7).
- Thakur, S.L., and Parmar, M., 2013. Adsorption of Heavy Metal (Cu²⁺, Ni²⁺ and Zn²⁺) from Synthetic Waste Water by Tea Waste Adsorbent. *International Journal of Chemical and Physical Sciences*, 2, 6–19.

- Wang, J., Zheng, S., Shao, Y., Liu, J., Xu, Z., and Zhu, D., 2010. Amino-Functionalized Fe₃O₄@SiO₂ Core-Shell Magnetic Nanomaterial as a Novel Adsorbent for Aqueous Heavy Metals Removal. *Journal of Colloid and Interface Science*, 349, 293–299. <https://doi.org/10.1016/j.jcis.2010.05.010>.
- Wijayanti, I.E., and Kurniawati, E.A., 2019. Studi Kinetika Adsorpsi Isoterm Persamaan Langmuir Dan Freundlich Pada Abu Gosok Sebagai Adsorben. *EduChemia (Jurnal Kimia dan Pendidikan)*, 4, 175. <https://doi.org/10.30870/educhemia.v4i2.6119>.
- Yuan, L., and Liu, Y., 2013. Removal of Pb(II) and Zn(II) from Aqueous Solution by Ceramisite Prepared by Sintering Bentonite, Iron Powder and Activated Carbon. *Chemical Engineering Journal*, 215–216, 432–439. <https://doi.org/10.1016/j.cej.2012.11.016>.
- Zhou, Q., Xing, A., and Zhao, K., 2014. Simultaneous Determination of Nickel, Cobalt and Mercury Ions in Water Samples by Solid Phase Extraction Using Multiwalled Carbon Nanotubes as Adsorbent after Chelating with Sodium Diethyldithiocarbamate Prior to High Performance Liquid Chromatography. *Journal of Chromatography A*, 1360, 76–81. <https://doi.org/10.1016/j.chroma.2014.07.084>.